

Research Article

Contactless Modal Phenomena Based Approach to Detecting, Identifying, and Diagnosing of Electrical Connections

Pavel Orlov  and Talgat Gazizov 

Tomsk State University of Control Systems and Radioelectronics, Lenin Ave. 40, Tomsk 634050, Russia

Correspondence should be addressed to Pavel Orlov; praetorian281@gmail.com

Received 11 January 2018; Revised 4 April 2018; Accepted 15 April 2018; Published 30 May 2018

Academic Editor: Gangbing Song

Copyright © 2018 Pavel Orlov and Talgat Gazizov. This is an open access article distributed under the Creative Commons Attribution License, which permits unrestricted use, distribution, and reproduction in any medium, provided the original work is properly cited.

This paper presents a unified description of a new approach for contactless detection, identification, and diagnostics of electrical connections and describes an idea and principles of using modal probing for these tasks. Simulation and experimental results on pulsed signal propagation through flat cables demonstrate the modal decomposition of a pulsed signal, which varies depending on the state of the probed wire. It is shown that the presented tasks can be solved by modal probing. The article also considers the analysis of modal distortions in frequency domain and gives the formula for its practical use. This formula can be useful when the pulse duration time is longer than the minimum of mode delay difference. In conclusion, we present further development ideas of the modal probing.

1. Introduction

To provide error-free and stable performance of electronic and electrical systems it is important to control their functioning. In this case, detection, identification, and diagnostics of electrical connections become urgent [1], especially for such areas as aeronautics and aerospace [2]. One of the ubiquitous techniques is reflectometry. The development of this technique increases its functionality and applications [3–5]. Unfortunately, the reflectometry response itself is not always self-sufficient to identify and locate the defects in the electrical connections and it is a reason why a solution of the inverse problem may also enhance the applicability of reflectometry [6, 7]. However, wiring network development strengthens the requirements for probing devices, which necessitates creation of the devices based on other principles. The impedance spectroscopy can be applicable for wire fault diagnostics [8, 9]. Particularly, the development of contactless methods is important [10].

A new device has already been suggested for contactless (hereinafter, the term “contactless” means no need for galvanic connection with the device under test) detection, identification, and diagnostics based on the idea of employing modal distortions of pulsed signal waveform [11]. However,

the practical implementation of the device requires careful investigation of the modal phenomena in multiwire structures. A number of theoretical studies have been carried out using the software for quasistatic and electromagnetic simulation showing the ability to apply modal phenomena for detecting, identifying, and diagnosing multiwire structures and to create devices based on these phenomena [12]. Moreover, there have been some experiments carried out to confirm that one pulse can be decomposed into several pulses with lower amplitudes because of different modal delays in the structure [13], with approaches to apply modal phenomena for protecting critical equipment against the effects of UWB-pulses propagation being described [14]. Experimental results on flat cable have demonstrated the possibility of contactless wire diagnostics using modal probing even without galvanic connection to the wire [15]. The obtained results have demonstrated the possibility of developing new devices for detecting, identifying, and diagnosing electrical connections. However, the implementation of the possibility requires analyzing the signal not only in time but also in frequency domains. The first steps of modal distortion analysis in frequency domain for contactless diagnostic of electrical connections have already been described [16]. Unfortunately, generalized presentation of the obtained and some new

results on modal probing is still absent. Meantime, it can be useful to reveal the promising ways of future work.

In this paper, a generalized description of possible applications of modal phenomena for contactless detection, identification, and diagnostics of electrical connections is given for the first time.

This paper is organized as follows: Section 2 presents the theoretical background of modal probing. Section 3 describes the simulation approaches used in this paper. Section 4 describes the use of modal probing for detecting and identifying electrical connections. The diagnostics opportunities are presented in Section 5, and the analysis of modal distortion in frequency domain is presented in Section 6. The paper is concluded in Section 7.

2. Modal Probing Background

It is known that during the propagation of the pulse signal along the N -conductor transmission line (conductor $N + 1$ is the reference one) in nonhomogeneous dielectric filling, the pulse signal may be subjected to modal distortions up to decomposition into N pulses of smaller amplitude due to different modal delays. Complete decomposition of the pulse signal in the line of length l will occur if the total duration t_Σ of exciting pulse is less than the minimum modulus among the differences of modal delays, that is, under condition [17]

$$t_\Sigma < l \min |\tau_i - \tau_k|, \quad i, k = 1, \dots, N, \quad i \neq k, \quad (1)$$

where $\tau_{i(k)}$ is per-unit-length delay for $i(k)$ -th mode of structure. Indeed, according to modal theory [18], a pulse excitation of the N -conductor transmission line is considered as combination of the pulse modes, propagating in the line with own per-unit-length delays (as well as other characteristics). Each of the delays multiplied by l will give the corresponding time when the pulse arrives at the line end. In case of small values of the time, the neighboring pulses can overlap. However, if the minimal of the values is more than the total duration of the exciting pulse then the overlapping of the mode pulses will be diminished until the pulses are completely decomposed at the line end. This phenomenon can be used for detecting, identifying, and diagnosing electrical connections. In this paper, generalization of these opportunities is called modal probing. If probed conductors have different electrical and magnetic couplings with the probing line, the information about probed conductors can be obtained from the waveform of modal distortions in the probing line.

A block diagram of the device that implements the principles of modal probing is shown in Figure 1. The device operates as follows: the probing pulse from the generator propagates along a probing line. This pulse undergoes modal distortions caused by the presence of probed conductors. A transmitted signal from the probing line output and a reflected signal from the probing line input go to the receiver inputs and then to the processing unit. All units of the device function according to control unit signals. Information about the probed structure is extracted from the waveforms at the near and far ends of the probing line.

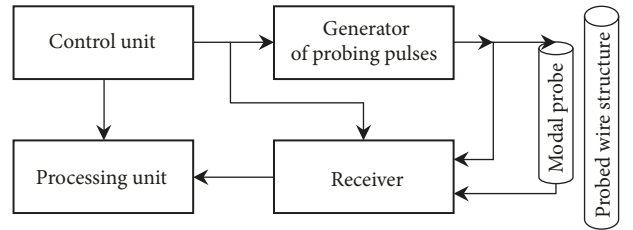


FIGURE 1: Block diagram of the modal probing device.

3. Simulation Approach

In this paper, the simulation of pulse propagation is carried out by electromagnetic and quasistatic approaches. The first is used for validation made on the basis of finite integration technique. The second is used as a main approach based on fast and accurate models implemented in the available TALGAT software [19]. The simulation is described below in more detail. The TALGAT software is based on the method of moments and allows us to make 2D quasistatic analysis. The algorithm implemented in the software allows calculating all elements of a moment matrix by using fully analytical formulae only, avoiding the time-consuming and approximate numerical integration. It can be useful for effective calculation of a capacitive matrix of 2D structures of various complexity. (Complete details of the algorithm are commonly available [20] and omitted here because of awkwardness.) We simulate a short pulse propagation along a multiconductor transmission line as a base of the structures under consideration. It is assumed in the analysis that a transmission line is uniform along its length with an arbitrary cross section. The cross section, in general, with N signal conductors and a reference, is represented by the following $N \times N$ matrices of line per-unit-length parameters: inductance (\mathbf{L}), coefficients of electrostatic induction (\mathbf{C}), resistance (\mathbf{R}), and conductance (\mathbf{G}). In paper [21] the approach based on a modified nodal admittance matrix has been presented to formulate network equations including multiconductor transmission lines, terminal, and interconnecting networks. We use the algorithm based on this approach and permitting to calculate the voltage not only at any node of the network but also at any point along any conductor of multiconductor transmission lines. (The algorithm details and various applications are not described here for the sake of brevity but can be found in [22–24].) It is the approach that is used in our research, and voltages in the time domain are obtained by applying the inverse fast Fourier transform.

4. Detection and Identification

By detection we mean the ability to detect passive (probed) conductors, while by identification we mean the ability to determine the amount of probed conductors and boundary conditions. The possibility of detecting and identifying electrical connections by modal probing is illustrated by quasistatic modeling of the trapezoidal pulse signal distortions in the microstrip structures with the length of 1.5 m (Figure 2).

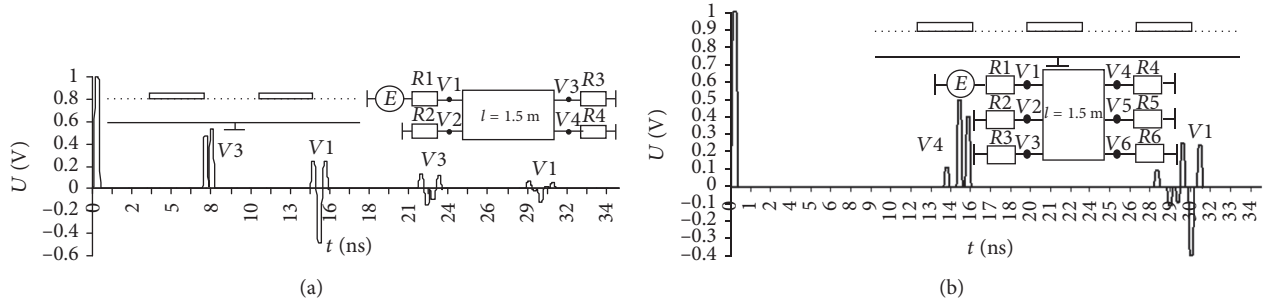


FIGURE 2: Voltage waveforms at the input and output of the microstrip line active conductor when (a) $N = 2$ and (b) $N = 3$.

TABLE 1: The matrices of the lines.

N	Matrices					
	L , nH/m			C , pF/m		
2	285	27		91	-3.8	
	27	285		-3.8	91	
3	284	27	7.2	91	-3.8	-0.05
	27	284	27	-3.8	91	-0.3
3	7.2	27	284	-0.05	-0.3	91

As the excitation source we chose a trapezoidal signal with EMF 2 V and the duration of rise, fall, and flat top of 0.1 ns. The boundary conditions at the ends of lines were chosen from the pseudomatching condition for active line and open circuit for others. The matrices of per-unit-length parameters are shown in Table 1. More detailed simulation setup and parameters of the structures are given in [17].

For $N = 2$ at the far end of the (active conductor) probing line (V3) there are two pulses instead of one (Figure 2(a)). The second pulse was caused by the presence of the probed passive conductor (and, as a consequence, by the excitation of even and odd modes), by its electric and magnetic couplings with the probing line and by the fact that the total duration of the input pulse is less than the total difference between mode delays. The difference of mode delays is caused by the inhomogeneous dielectric filling of the structure. For $N = 3$ at the far end of the probing line (V4) there are three pulses instead of one (Figure 2(b)). The appearance of three pulses is caused by the presence of two passive conductors, so three modes are excited in the structure and the delay difference between them is more than the pulse duration.

To confirm the possibility of using modal phenomena to detect electrical connections, we have carried out an experiment with the experimental PCB structure. The cross section and the photography of the experimental PCB are shown at Figure 3 and its parameters are presented in Table 2. The value of the resistance at the ends of lines with the length of 0.33 m during the experiment is 50Ω (R1–R4 on the schematic diagram in Figure 2(a)).

The experimental setup was based on a stroboscopic oscilloscope S9–11 (50Ω internal impedance, 17.8 GHz bandwidth) comprising a signal analyzer, an indicator, a generator,

a stroboscope, and a pulse shaper (Figure 4). A 20 dB attenuator was connected to the stroboscope input to protect it. The cable was connected to the pulse shaper and the attenuator via SMA connectors.

Each experiment was conducted in the following order. First, the UWB pulse from the pulse shaper propagated to an input connector, then directly (without the device under test) to the output connector, and, finally, to the attenuator and the stroboscope input to measure the signal waveform. Afterwards, the PCB or cable under test (DUT) was connected between the input and output connectors and the resulting signal waveform was measured. This experimental setup applies to all measurements with S9–11.

A voltage pulse was applied between the active trace and the reference planes of the experimental PCB. The signal parameters at the pulse shaper output under 50Ω load are listed in Table 3. The photography of the oscilloscope S9–11 with the measured input and output voltage waveforms is shown in Figure 5(a). (The input pulse was measured with a 20 dB attenuator, while other pulses were measured without it.) The comparative analysis of measured and simulated (by electromagnetic approach based on FIT method) voltage waveforms (Figure 5(b)) shows good coincidence.

Thus, these results show that according to the number of pulses at the far end of the active conductor we can determine the presence and the amount of passive conductors, that is, to solve the problem of detecting and identifying electrical connections.

Let us consider the possibility of modal probing for flat cables (Figure 6). The parameters of typical flat cables are presented in Tables 4–6. The data show that cables with air gaps have the difference of mode per-unit-length delays of more than 0.3 ns/m and cables without air gaps 0.5 ns/m. Therefore, modal probing is applicable for such cables.

To confirm the possibility of using modal phenomena to detect electrical connections, we carried out an experiment using S9–11 oscilloscope. The parameters of pulsed signals were measured at the near and far ends of the probing pair of the PUGNP 3×1.5 cable wires (Figure 6(a)), where **A** represents the active wire, **R** the reference wire, and **P** the passive wire. Thus, we considered the possibility of passive wire probing (without contact with it), based on the signal between the active and reference wires of the probing pair.

A voltage pulse was applied between the active and reference wires (a schematic diagram of the structure under

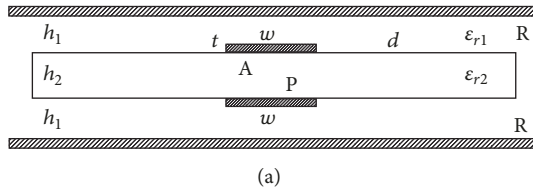


FIGURE 3: The cross section of the experimental PCB (a); photography of the experimental PCB with the scalar network analyzer P2M-40 connected to it (b).

TABLE 2: Parameters of the experimental structure.

$w, \mu\text{m}$	$t, \mu\text{m}$	$h_2, \mu\text{m}$	Parameters				Matrices			
			$h_1, \mu\text{m}$	ϵ_{r1}	ϵ_{r2}	$\Delta\tau, \text{ns/m}$	$L, \text{nH/m}$	$C, \text{pF/m}$	Z, Ω	
185	35	130	600	4.25	10.2	2.2	524.7 310.9	243.4 -179.5	68 46	
							310.9 524.7	-179.5 243.4	46 68	

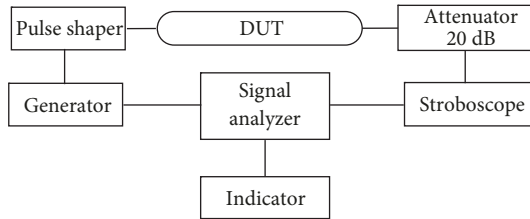


FIGURE 4: Schematic diagram of the experimental setup.

TABLE 3: Signal parameters at the pulse shaper output.

Signal type	Triangular pulse
Amplitude	320 mV
Rise time (0.1–0.9)	340 ps
Fall time (0.1–0.9)	340 ps
Duration (0.5)	240 ps

study is similar to that shown in Figure 2(a), but the length of the line (l) is 15 m) through the pulse shaper (with the output resistance $R1 = 50 \Omega$ and the maximum signal amplitude of 10 V). The input resistance of the oscilloscope was $R3 = 50 \Omega$, while $R2$ and $R4$ were changed: open circuit, short circuit, and 100Ω . The signal parameters at the pulse shaper output under 50Ω load are listed in Table 7, and the waveform is shown in Figure 7(a). (The input pulse was measured with a 20 dB attenuator, while other pulses were measured without it.)

The waveforms at the far end of the probing line are shown in Figure 7. Pulse amplitudes for different boundary conditions at the ends of the probed wire are presented in Table 8. In all these cases, there are two pulses instead of one at the far end of the probing line. The second pulse was caused by the presence of the probed passive conductor (and, as

a consequence, by the excitation of even and odd modes), by its electric and magnetic couplings with the probing line, and by the fact that the total duration of the input pulse ($\approx 0.6 \text{ ns}$) is less than the total difference between mode delays ($0.32 \text{ ns/m} \times 15 \text{ m} = 4.8 \text{ ns}$), as follows from Table 6. The oscilloscope pattern with the waveforms at the far end of the probing line (Figure 7(b)) with open circuit at the passive wire shows the ability to detect the conductor without any contact with it. To determine the boundary conditions at the ends of the passive conductor, the pulse shape should vary depending on the boundary conditions. There are two pulses at far end of the line in all oscilloscope patterns but their amplitudes depend on boundary conditions (Table 8).

Theoretical background of this dependence is based on modal theory and consists in the following. The resulting voltages and currents in the transmission lines under consideration are represented as superposition of voltages or currents of two decoupled transmission lines, having intrinsic characteristic impedance and per-unit-length delays, defined by even and odd modes. First, the exciting signal is represented as superposition of even and odd modes excitations. Then, each of the lines is excited by the intrinsic excitation. The resulting output voltage depends on transmission coefficients at the beginning and the end of a line. These coefficients are defined by boundary conditions and characteristic impedance of the modes. In case of pulse excitation, the resulting output voltage consists of two (even and odd modes) pulses of different amplitudes. In general, the values of the amplitudes are different, because they are defined by different transmission coefficients of the modes. The change of boundary conditions changes the resulting output voltages of even and odd pulses. Analytical expressions for transmission coefficients and pulse amplitudes can be easily derived similarly to [25]. However, this approach does not take into account the losses and dispersion, which may significantly

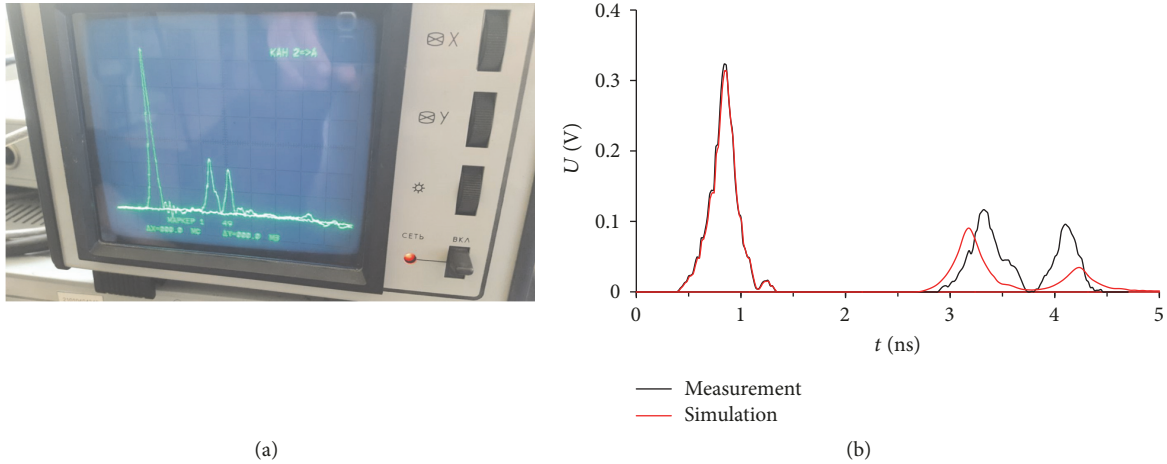


FIGURE 5: Photography of the oscilloscope S9-11 with measured input and output voltage waveforms (a); comparison of measured and simulated voltage waveforms (b) for the experimental PCB.

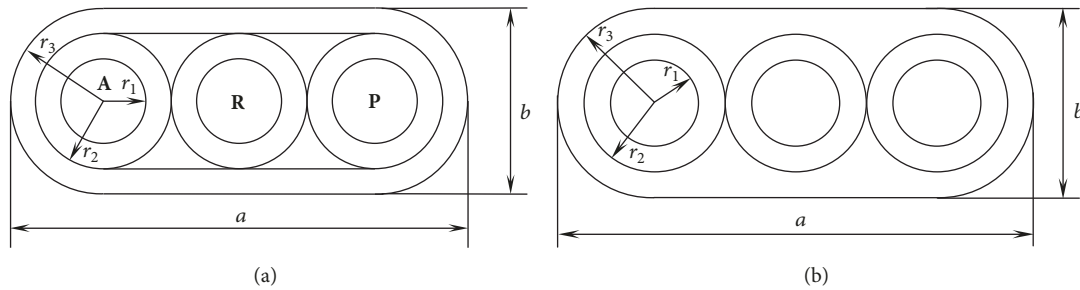


FIGURE 6: Cross section of cables with (a) and without (b) air gaps.

affect the amplitudes of the pulses. Therefore, numerical full-wave or above-mentioned quasistatic analysis is more relevant.

To verify the results of the experiment, we accomplished the quasistatic simulation. The results of the simulation are shown in Figure 8. For clarity, the comparison of the experiment and simulation results for open circuit case is shown in Figure 9. As we can see, the qualitative ratio between pulse amplitudes in the experiment and the simulation is similar, but the values of the amplitudes and the fall time are greater in the experiment. These differences are due to the difference of the actual and simulation parameters (of input signal, dielectrics, conductors, and boundary conditions), as well as measurement and simulation errors. The noncausal waveform of the simulation result is explained by ignoring the frequency dependence of ϵ_r and $\text{tg}\Delta$ during the simulation process. This effect is considered in detail in [26]. However, more detailed simulation and explanations of these results are out of the scope of this paper.

Thus, the results of the experiments and the simulations for cable of PUGNP 3×1.5 type confirm the possibility of detecting and identifying boundary conditions at the ends of a conductor by modal probing without electrical connection to the conductor. It is worth noting that none of the existing and utilized ways (pulse reflectometry, device-based induction methods) has such possibility.

5. Diagnostics

By diagnostics we mean the ability to determine passive (probed) conductor breaks. To diagnose a passive conductor with modal probing, the form of a modal distortion of the pulse signal should vary depending on the condition of the passive conductor. It is illustrated by the simulation of the pulse propagation along the flat cable of PUGNP 3×4 type (Figure 6(b)). We simulated two cases, with and without a break in a passive wire. The case with the break in the passive wire was simulated by using two sections of the cable (Figure 10), with $R_3 = R_4 = 5 \text{ G}\Omega$. The total length of the structure was equal to 2 m, and the point of the passive wire break was moved over the distances of 0.5, 1, and 1.5 m from the near end of the passive wire. (The probing pulse parameters are EMF amplitude 2 V; each of rise, fall, and flat top time values is 100 ps). The simulation results are shown in Figure 11.

Simulation results show that, in the case without a break of a passive wire (Figure 11(a)), two pulses instead of one come to the far end of the probing line, and the reason why they occur was described above. With the passive wire break, the number of pulses at the end of the probing line increases (Figures 11(b)–11(d)). When the break point is located at the distance of 0.5 m from the near end of the structure, the number of pulses at the far end of the probing line doubles. This is due to the fact that at the passive wire break point the

TABLE 4: Geometrical (mm) and material parameters of cables with air gaps.

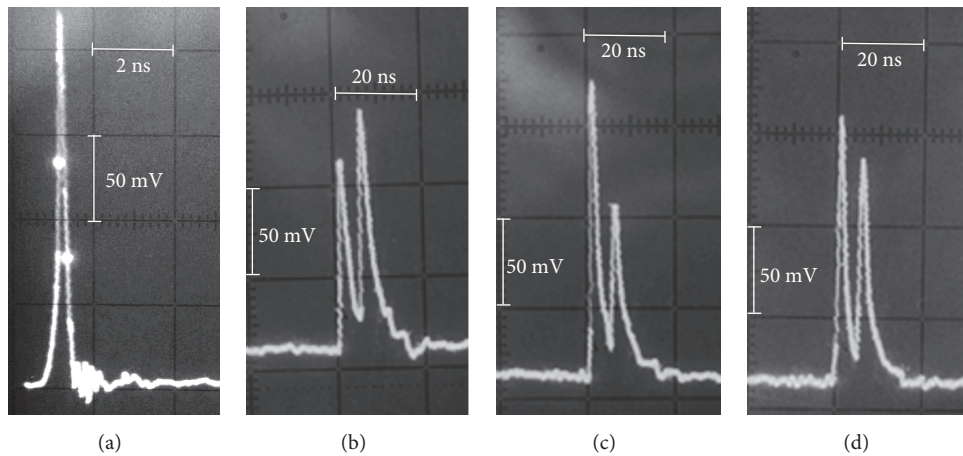
Cable type	Parameters				Material	
	Wire radii (r_1)	Wire isolation radii (r_2)	Cable isolation radii (r_3)	Cable size ($a \times b$)	Conductor	Dielectric
VVG 3 \times 1.5	0.690	1.200	2.055	8.89 \times 4.11	Cu	PVC
VVG 3 \times 2.5	0.892	1.350	2.160	10.02 \times 4.32	Cu	PVC
VVG 3 \times 4	1.128	1.825	2.875	12.97 \times 5.75	Al	PVC
PUGNP 3 \times 1.5	0.690	1.175	1.950	8.40 \times 3.90	Cu	PVC

TABLE 5: Geometrical (mm) and material parameters of cables without air gaps.

Cable type	Parameters				Material	
	Wire radii (r_1)	Wire isolation radii (r_2)	Cable isolation radii (r_3)	Cable size ($a \times b$)	Conductor	Dielectric
PUGNP 3 \times 2.5	0.892	1.375	2.000	9.60 \times 4.00	Cu	PVC
PUGNP 3 \times 4	1.128	1.600	2.275	11.50 \times 4.55	Cu	PVC

TABLE 6: L, C, and Z matrixes, mode per-unit-length delays, and their difference for the cables under consideration.

Cable type	Matrixes						Per-unit-length delays, ns/m		
	L, nH/m		C, pF/m		Z, Ω		τ_e	τ_o	$\Delta\tau$
VVG 3 \times 1.5	458.53	111.59	55.56	-10.09	94.40	60.16	5.090	4.777	0.313
	111.59	458.53	-10.09	55.56	60.16	94.40			
VVG 3 \times 2.5	387.65	83.41	62.22	-9.63	81.21	48.59	4.977	4.676	0.302
	83.41	387.65	-9.63	62.22	48.59	81.21			
VVG 3 \times 4	422.48	96.73	58.64	-9.56	87.62	53.86	5.048	4.713	0.335
	96.73	422.48	-9.56	58.64	53.86	87.62			
PUGNP 3 \times 1.5	448.25	106.95	56.05	-9.88	92.74	58.51	5.063	4.743	0.320
	106.95	448.25	-9.88	56.05	58.51	92.74			
PUGNP 3 \times 2.5	397.04	86.94	73.81	-8.90	74.88	43.08	5.602	5.063	0.539
	86.94	397.04	-8.90	73.81	43.08	74.88			
PUGNP 3 \times 4	351.63	70.29	82.82	-8.65	66.19	36.14	5.594	5.073	0.521
	70.29	351.63	-8.65	82.82	36.14	66.19			

FIGURE 7: Oscilloscope waveforms of input signal (a) and signal at the far end of the probing line (V4) with open circuit (b), short circuit (c), and 100 Ω (d) at both ends of the probed conductor.

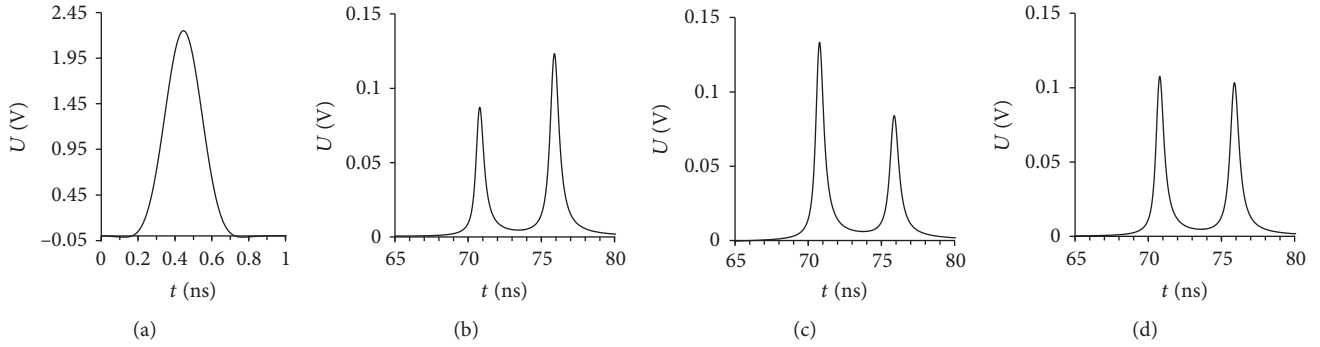


FIGURE 8: Simulated waveforms of input signal (a) and signal at the far end of the probing line (V_4) with open circuit (b), short circuit (c), and $100\ \Omega$ (d) at both ends of the probed conductor.

TABLE 7: Signal parameters at the pulse shaper output.

Signal type	Triangular pulse
Amplitude	225 mV
Rise time (0.1–0.9)	280 ps
Fall time (0.1–0.9)	280 ps
Duration (0.5)	200 ps
Horizontal scale division	2 ns/div
Vertical scale division	50 mV/div

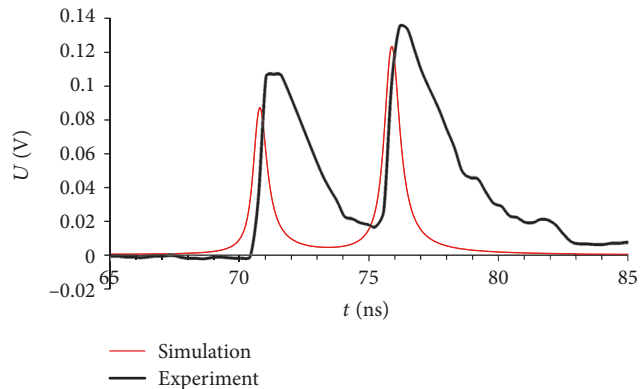


FIGURE 9: Comparison of simulated and experimental results of waveforms at the far end of the probing line (V_4) with open circuit at both ends of the probed conductor.

pulse is decomposed into two pulses because the difference of modal delays in line 1 is more than the probing pulse duration. When the break point is located at the distance of 1 m from the near end of the structure, there are three pulses at the far end of the probing line; the pulses are overlapped, so the middle pulse amplitude is rising. Thus, the information obtained from the waveform at the far end of the probing line allows us to determine a break of the passive wire. Reflections at the near end of the probing line are also informative because they allow us to locate the break.

Moreover, we obtained the experimental results confirming the diagnostics with the use of modal probing. To research the possibilities of the passive wire break diagnostics, we performed the experiment on two structures shown in

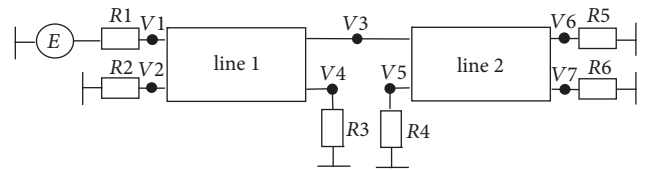


FIGURE 10: Schematic diagram of the structure under study with the break in the passive wire.

Figures 2(a) and 10. The electrical parameters of the considered cable (PUGNP 3×1.5) are presented in Table 6. The experimental conditions are thoroughly described in Section 4.

The oscillograms of the source signal and the signal at the far end of the probing line for the structure without a passive wire break (Figure 2(a)), when $R2 = R4 = 100\ \Omega$, are shown in Figure 12. The measured time delay of the fastest mode (considering the maximum permissible error of 7.5% with horizontal scale division 20 ns/div for S9–11 oscilloscope) is 72 ± 5.4 ns, which corresponds to the per-unit-length delay τ_o (Table 6) multiplied by the structure length (4.74 ns/m \times 15 m = 71.1 ns). The appearance of the second pulse is due to the presence of a passive (probed) wire, as well as to the fact that the total duration of the initial pulse (≈ 0.6 ns) is less than the full difference of the mode delay (0.32 ns/m \times 15 m = 4.8 ns), as follows from Table 6. Waveforms at the far end of the probing line under various boundary conditions at the ends of the passive wire are omitted here but were considered in more detail in [12].

The waveform at the far end of the probing line for the case with the passive wire break is shown in Figure 13(a). As can be seen, when passive wire is broken, four pulses come to the far end of the probing line instead of two pulses, as in the case without the break. The partial overlap of the pulses is due to dispersion. The reflected signal caused by the presence of the break in the passive conductor is observed too (it is circled in a white frame). The delay difference between transmitted and reflected signals is approximately 48 ± 3.6 ns (horizontal scale division 20 ns/div.) and corresponds to the per-unit-length delay τ_o (from Table 6) multiplied by twice the length of the line 1 (4.74 ns/m \times 2×5 m = 47.4 ns). Thus, the change in the number of pulses at the far end of the probing

TABLE 8: Pulse amplitudes for different boundary conditions at the ends of the probed wire for experiment and simulation.

Boundary conditions	Pulse 1, mV		Pulse 2, mV	
	Experiment	Simulation	Experiment	Simulation
Open circuit	112	85	133	121
Short circuit	160	131	93	82
100 Ω	148	107	124	101

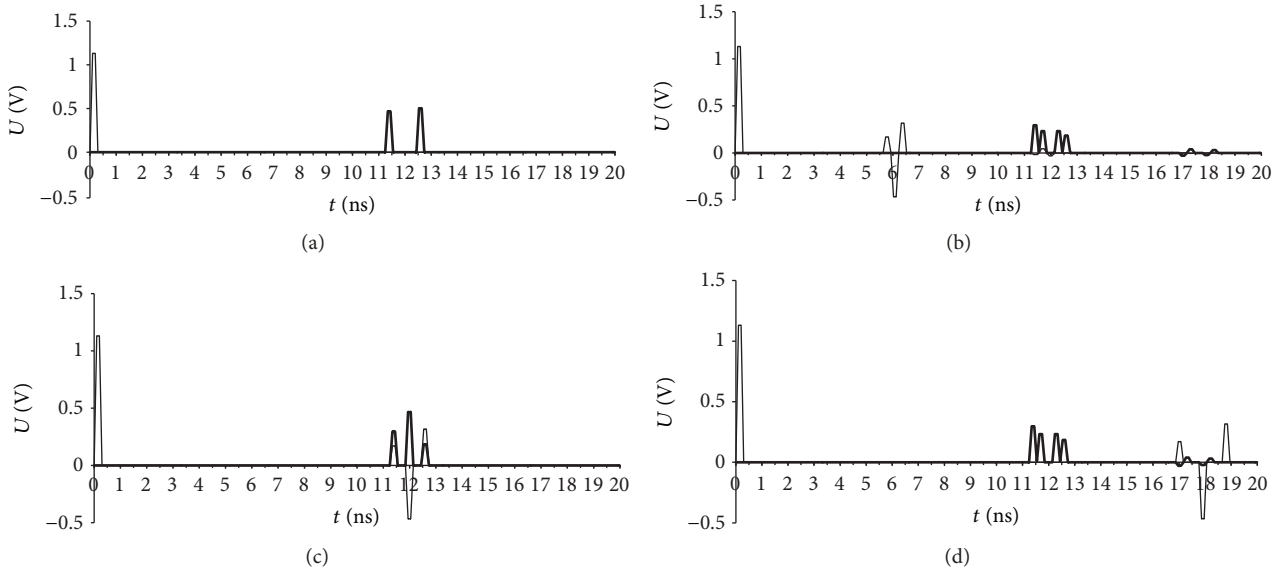
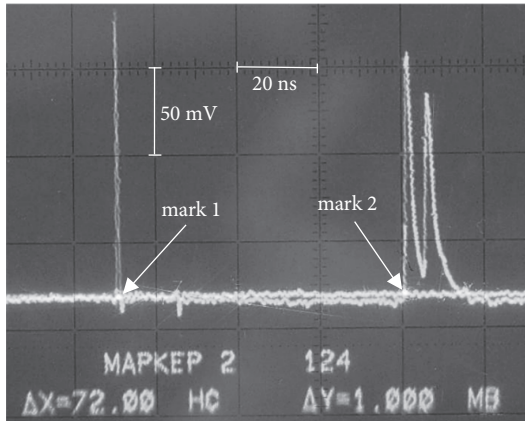


FIGURE 11: Simulated waveforms at the near (—) and far (---) ends of the probing line without the break of the passive wire (a) and with its break at distances of 0.5 (b), 1 (c), and 1.5 (d) m from the beginning.

FIGURE 12: Oscillograph pattern of a source signal (with 20 dB attenuator) and a signal at the far end of the probing line (V4) for the structure (without attenuator) from Figure 2(a) when $R_2 = R_4 = 100 \Omega$.

line experimentally confirms the possibility of contactless diagnostics of wire structures by modal probing, while the reflected signal may help to locate the wire break.

The case when there is no galvanic connection between the probing line and passive wire (i.e., open circuit condition holds at both ends of the passive wire) is of practical interest. The waveform at the far end of the probing line for this case

is shown in Figure 13(b). As in the case of 100Ω , four pulses are observed at the far end of the probing line. Thus, the presented waveforms indicate the possibility of wire break diagnostics by modal probing in the case when there is no galvanic connection either. It is noteworthy that the change in the boundary conditions at the ends of the passive wire leads to a change in the amplitude of pulses. The simulation results for this case ($R_2 = R_4 = \infty$) are shown in Figure 14. These results are consistent with the experiment and more clearly demonstrate that there are 4 pulses at the far end. Time delay between transmitted and reflected signals ($116 \text{ ns} - 69 \text{ ns} = 47 \text{ ns}$) is also consistent with the experiment (47.4 ns).

6. Analysis of the Modal Distortions in the Frequency Domain

Modal decomposition will occur only under the condition (1). However, when decomposed pulses are considerably overlapping, it becomes difficult to detect the decomposition fact when analyzing modal distortions in the time domain only. One of the approaches to solve this problem is the additional analysis in the frequency domain [16].

Frequency of the first minimum in a spectrum of a signal at the far end of an active conductor of a matched multiconductor transmission line is obtained with the following expression:

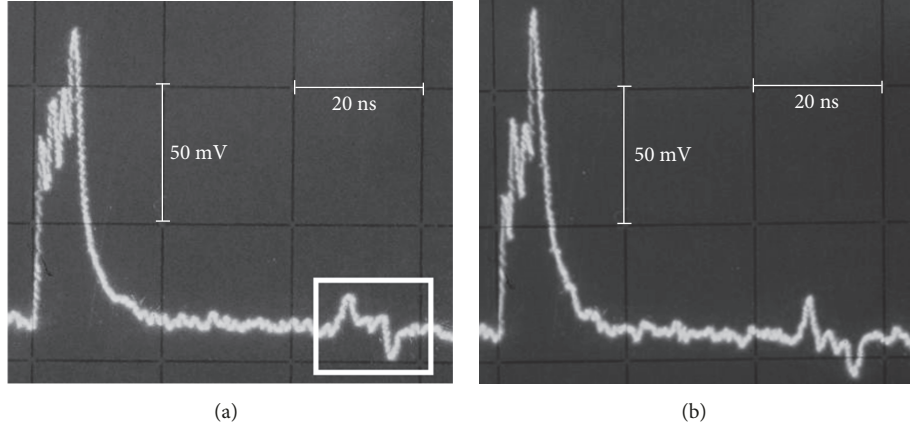


FIGURE 13: Waveform at the far end of the probing line (V_4) of the structure with a passive wire break when $R_2 = R_4 = 100 \Omega$ (a) and $R_2 = R_4 = \infty$ (b).

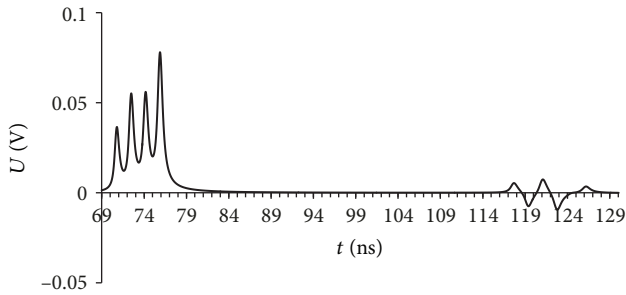


FIGURE 14: Simulated waveform at the far end of the probing line (V_4) of the structure with a passive wire break when $R_2 = R_4 = \infty$.

$$f_0 \approx \frac{1}{2l(\max(\tau_i) - \min(\tau_i))}, \quad i = 1, 2, \dots, N, \quad (2)$$

where l is length of a structure, τ_i is a per-unit-length delay for i -th mode of a structure, and N is the number of wires (excluding a reference one). For $N = 2$ (2) takes the form

$$f_0 = \frac{1}{2l|\tau_e - \tau_o|}, \quad (3)$$

where τ_e and τ_o are per-unit-length delays for even and odd modes. Then from (3) we obtain

$$l = \frac{1}{2f_0|\tau_e - \tau_o|}. \quad (4)$$

Now, using (4), we can determine the distance to the wire break point. It can be confirmed by the experimental results in a time domain described in detail above. The waveform and the spectrum of the signal at the far end of the probing line for the structure (of total length 15 m) without the passive wire break are shown in Figure 15, and with the break (at 5 m from the near end) in Figure 16. From Figure 15(a) it is possible to find the difference between the mode delays through the delay difference between the two pulse peaks ($20 \text{ ns/div.} \times 0.26 \text{ div.} = 5.2 \text{ ns}$). Then the per-unit-length delay difference would be 0.35 ns/m .

Let us refer to the data in the frequency domain. Taking the first frequency of the minimum value (83 MHz) measured by markers (Figure 15(b)) in the spectrum, we obtain (4)

$$l = \frac{1}{2 \cdot 83 \text{ MHz} \cdot 0.35 \text{ ns/m}} = 17.2 \text{ m}. \quad (5)$$

The difference between the calculated (17.2 m) and real (15 m) length values is $\pm 7\%$. Similarly, for the structure with a break (Figure 16(b)) we obtain (4)

$$l = \frac{1}{2 \cdot 126.9 \text{ MHz} \cdot 0.35 \text{ ns/m}} = 11.25 \text{ m}. \quad (6)$$

The difference between the calculated (11.25 m) and real (10 m) length values is $\pm 6\%$. For structures with a wire break, (4) gives the longest segment length. The difference between the real and calculated values is caused by a measurement error.

Consistency of experimental and simulated results is observed not only in time but also in the frequency domain. The simulation results of signal spectrum at the far end for the cases with and without a wire break are shown in Figure 17. There is a slight difference between the first resonance frequencies in comparison with the experiment (Figures 15 and 16). The values of these frequencies and their differences in the percentage terms are given in Table 9. The reasons of these differences are similar to the ones described in Section 4.

A similar experiment was conducted for the experimental PCB. However, the measurements were carried out with the scalar network analyzer R2M-40 (50Ω internal impedance, 40 GHz band-width). The experimental setup is shown in Figure 18. We measured S-parameters. The measured and simulated frequency dependencies of $|S_{21}|$ are shown in Figure 19. Taking the first frequency of the $|S_{12}|$ minimum (545 MHz) measured by R2M-40 (Figure 19), we obtain (4)

$$l = \frac{1}{2 \cdot 545 \text{ MHz} \cdot 2.2 \text{ ns/m}} = 0.41 \text{ m}. \quad (7)$$

The difference between the calculated (0.41 m) and real (0.33 m) length values is $\pm 11\%$.

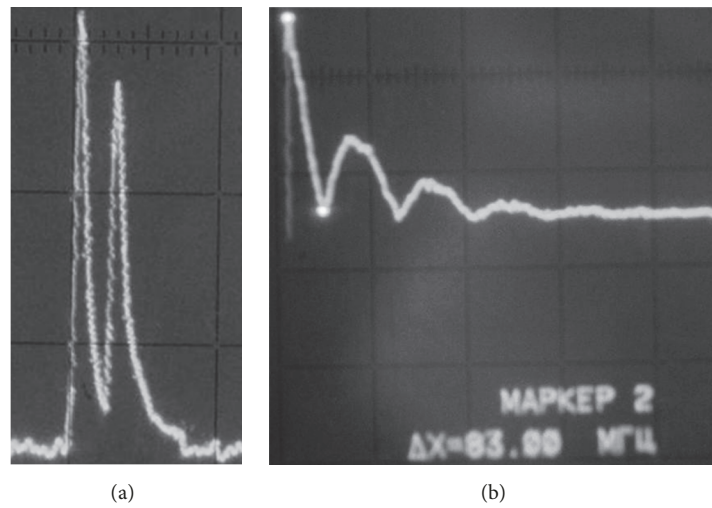


FIGURE 15: The waveform (a) and the spectrum (b) of the signal at the far end of a structure without a wire break.

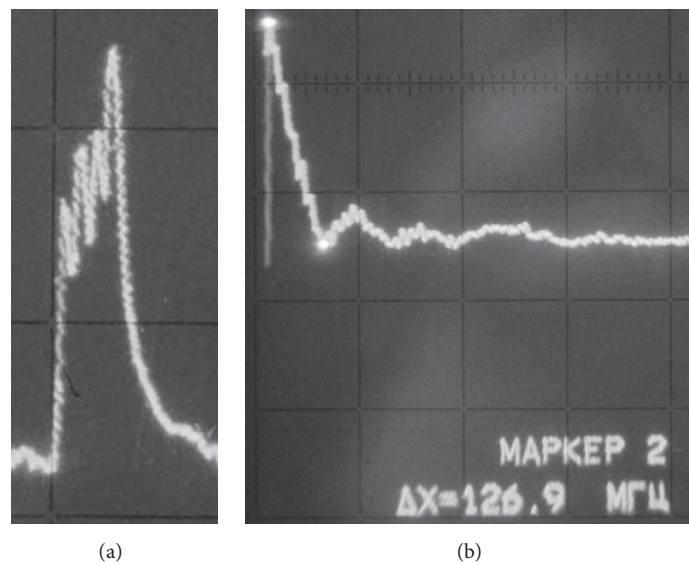


FIGURE 16: The waveform (a) and the spectrum (b) of the signal at the far end of a structure with a wire break.

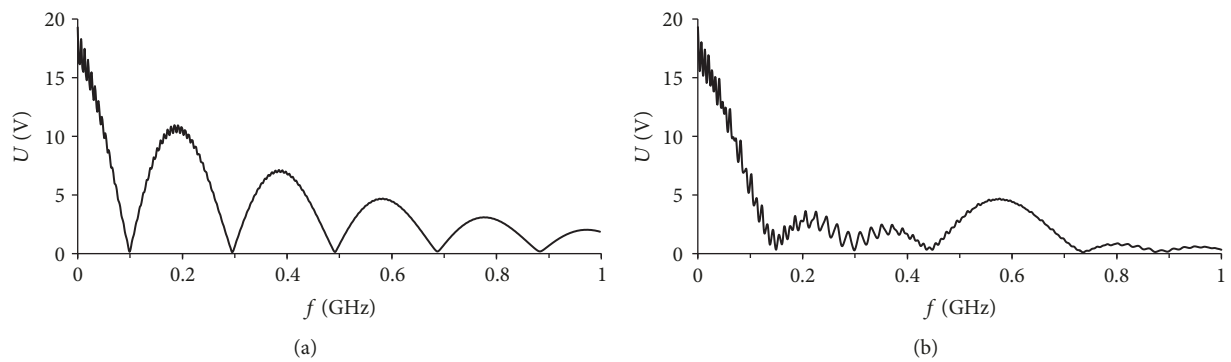


FIGURE 17: Simulated spectrum of the signal at the far end of a structure without (a) and with (b) wire break.

TABLE 9: Calculated and measured values of the first resonance frequency spectrum of the signal.

Case	First resonance frequency, MHz		$(f_S - f_E) / (f_S + f_E) \cdot 100\%$
	Simulation	Experiment	
Without a break	96.7	83	$\pm 7.6\%$
With a break	135	127	$\pm 3.05\%$

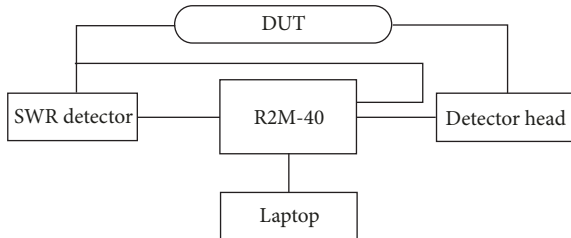
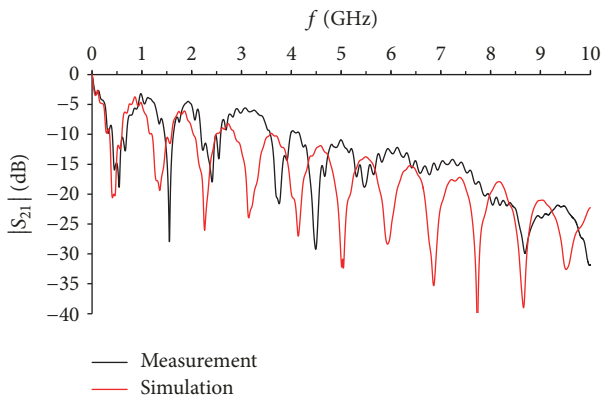


FIGURE 18: Schematic diagram of the experimental setup.

FIGURE 19: The measured and simulated frequency dependencies of $|S_{21}|$ for the experimental PCB.

Thus, the experimental and simulated results have allowed us to test the formula that relates the length of the longest segment of a structure with the difference of modal delays and the frequency of the first minimum in the spectrum of the signal at the far end of the structure. It can be used to diagnose electrical connections. Therefore, the results indicate the possibility of applying frequency analysis in modal probing.

7. Conclusion

In this paper, we described the principles of employing modal phenomena to detect, identify, and diagnose electrical connections. The proposed approach is based on a complex analysis of signal modal distortion and has two principal advantages: firstly, the galvanic connection to the probed line is not necessary and, secondly, the informativeness is inherent in other methods requiring the connection to the probed line (e.g., pulse reflectometry).

The results of the simulations and the experiments have confirmed the possibility of using modal probing. The first steps in the research of modal distortions in the frequency domain have yielded a formula that permits us to find the

length of the longest segment in the structure and the existence of a wire break in the structure, even when condition (1) is not fulfilled and there is no complete modal decomposition. However, it is required to pursue more in-depth research into applying modal phenomena for detecting, identifying, and diagnosing electrical connections by modal probing.

It should be noted that this paper does not fully describe the modal probing possibilities. Particularly, further development of the method requires a detailed research into modal distortion for structures with $N > 2$. Moreover, research into the effect of lumped elements along passive conductors on modal distortion is also high-potential. Simulation, design, and implementation of models and prototypes for various options of devices based on the modal probing are necessary to take its benefits.

Data Availability

The data used to support the findings of this study are available from the corresponding author upon request.

Disclosure

All authors are with Department of Television and Control of Tomsk State University of Control Systems and Radioelectronics, Tomsk, Russia.

Conflicts of Interest

The authors declare that there are no conflicts of interest regarding the publication of this paper.

Acknowledgments

This research was supported by the Ministry of Education and Science of the Russian Federation (Project 8.9562.2017/8.9).

References

- [1] F. Auzanneau, "Wire troubleshooting and diagnosis: review and perspectives," *Progress in Electromagnetics Research B*, vol. 49, pp. 253–279, 2013.
- [2] M. W. Stavnes and A. N. Hammoud, "Assessment of Safety in Space Power Wiring Systems," *IEEE Aerospace and Electronic Systems Magazine*, vol. 9, no. 1, pp. 21–27, 1994.
- [3] A. Lelong, L. Sommervogel, N. Ravot, and M. O. Carrion, "Distributed reflectometry method for wire fault location using selective average," *IEEE Sensors Journal*, vol. 10, no. 2, pp. 300–310, 2010.
- [4] W. Ben Hassen, F. Auzanneau, F. Peres, and A. P. Tchangani, "Diagnosis sensor fusion for wire fault location in CAN bus

- systems,” in *Proceedings of the 12th IEEE Sensors Conference*, pp. 1–4, IEEE, Baltimore, MD, USA, November 2013.
- [5] S. Naik, C. M. Furse, and B. Farhang-Boroujeny, “Multicarrier reflectometry,” *IEEE Sensors Journal*, vol. 6, no. 3, pp. 812–818, 2006.
 - [6] M. K. Smail, L. Pichon, M. Olivas, F. Auzanneau, and M. Lambert, “Detection of defects in wiring networks using time domain reflectometry,” *IEEE Transactions on Magnetics*, vol. 46, no. 8, pp. 2998–3001, 2010.
 - [7] S. Schuet, D. Timuçin, and K. Wheeler, “A model-based probabilistic inversion framework for characterizing wire fault detection using TDR,” *IEEE Transactions on Instrumentation and Measurement*, vol. 60, no. 5, pp. 1654–1663, 2011.
 - [8] Q. Shi and O. Kanoun, “Automated wire fault location using impedance spectroscopy and genetic algorithm,” in *Proceedings of the 2012 IEEE Sensor Conference*, pp. 1–4, Taipei, Taiwan, October 2012.
 - [9] Q. Shi and O. Kanoun, “Automated wire fault location using impedance spectroscopy and Differential Evolution,” in *Proceedings of the 2013 IEEE International Instrumentation and Measurement Technology Conference (I2MTC '13)*, pp. 359–364, IEEE, Minneapolis, MN, USA, May 2013.
 - [10] S. Wu, C. Furse, and C. Lo, “Noncontact probes for wire fault location with reflectometry,” *IEEE Sensors Journal*, vol. 6, no. 6, pp. 1716–1721, 2006.
 - [11] T. R. Gazizov, P. E. Orlov, A. M. Zabolotsky et al., “The device detection, identification and diagnosis of multiconductor transmission lines,” *RF Patent*, Article ID 2386964, 2009.
 - [12] P. E. Orlov and T. R. Gazizov, *New Approaches to Improve The Electrical Connections of Spaceborne Equipment*, p. 184, Tomsk, Russia, 2013.
 - [13] T. R. Gazizov, A. M. Zabolotsky, and I. E. Samotin, “Experimental results on ultra wide band pulse propagation in three-conductor power cables of flat and circular cross sections,” in *Proceedings of the International Siberian Conference on Control and Communications (SIBCON'09)*, pp. 264–269, IEEE, Tomsk, Russia, March 2009.
 - [14] T. R. Gazizov, A. M. Zabolotsky, A. O. Melkozerov, E. S. Dolganov, and P. E. Orlov, “Improved design of modal filter for electronics protection,” in *Proceedings of the 2012 International Conference on Lightning Protection (ICLP)*, pp. 1–4, Vienna, Austria, September 2012.
 - [15] P. E. Orlov, T. R. Gazizov, and A. M. Zabolotsky, “Experimental confirmation of the possibility for contactless diagnostics of multiconductor structures using modal probing,” *Russian Physics Journal*, vol. 56, no. 6, pp. 652–656, 2013.
 - [16] P. E. Orlov, T. R. Gazizov, and A. M. Zabolotsky, “Frequency analysis of modal distortions and its application to diagnostics of electric connections,” *Russian Physics Journal*, vol. 56, no. 9, pp. 1099–1101, 2014.
 - [17] A. M. Zabolotsky, T. R. Gazizov, A. G. Bova, and W. A. Radasky, “Dangerous pulse excitation of coupled lines,” in *Proceedings of the 17th International Zurich Symposium on Electromagnetic Compatibility*, pp. 164–167, IEEE, Singapore, February 2006.
 - [18] C. R. Paul, *Analysis of Multiconductor Transmission Lines*, p. 780, Wiley-IEEE Press, 2nd edition, 2007.
 - [19] S. Kuksenko, T. Gazizov, A. Zabolotsky et al., “New developments for improved simulation of interconnects based on method of moments/advances in intelligent systems research (ISSN 1951-6851),” in *Proceedings of the 2015 International Conference on Modeling, Simulation and Applied Mathematics (MSAM'15)*, pp. 293–301, Phuket, Thailand, August 2015.
 - [20] T. R. Gazizov, “Analytic expressions for MOM calculation of capacitance matrix of two dimensional system of conductors and dielectrics having arbitrarily oriented boundaries,” in *Proceedings of the 2001 International Symposium on Electromagnetic Compatibility (EMC 2001)*, pp. 151–155, IEEE, Montreal, Que., Canada, 2001.
 - [21] J. R. Griffith and M. S. Nakhla, “Time-Domain Analysis of Lossy Coupled Transmission Lines,” *IEEE Transactions on Microwave Theory and Techniques*, vol. 38, no. 10, pp. 1480–1487, 1990.
 - [22] R. R. Gazizov, A. M. Zabolotsky, and T. R. Gazizov, “Ultrashort pulse maximum localization in multiconductor structures,” in *Proceedings of the 2016 Dynamics of Systems, Mechanisms and Machines, Dynamics 2016*, pp. 1–5, IEEE, Omsk, Russia, November 2016.
 - [23] R. R. Gazizov, A. O. Belousov, and T. R. Gazizov, “Influence of ultrashort pulse duration on localization of crosstalk peak values in PCB of spacecraft autonomous navigation system,” in *Proceedings of the 2017 International Siberian Conference on Control and Communications, SIBCON 2017*, pp. 1–6, IEEE, Astana, Kazakhstan, June 2017.
 - [24] R. R. Gazizov, R. S. Ryabov, and T. T. Gazizov, “Influence of crossover and mutation coefficients on GA optimization of ultrashort pulse duration by criteria of peak voltage maximization in PCB bus,” in *Proceedings of the 2017 International Multi-Conference on Engineering, Computer and Information Sciences (SIBIRCON)*, pp. 415–420, Novosibirsk, September 2017.
 - [25] S. Park, F. Xiao, and Y. Kami, “Analytical approach for crosstalk characterization of multiconductor transmission lines using mode decomposition technique in the time domain,” *IEEE Transactions on Electromagnetic Compatibility*, vol. 52, no. 2, pp. 436–446, 2010.
 - [26] A. R. Djordjević, R. M. Biljić, V. D. Likar-Smiljanić, and T. K. Sarkar, “Wideband frequency-domain characterization of FR-4 and time-domain causality,” *IEEE Transactions on Electromagnetic Compatibility*, vol. 43, no. 4, pp. 662–667, 2001.



Hindawi

Submit your manuscripts at
www.hindawi.com

